"EFFECT OF TEMPERATURE ON CO_2 CORROSION BEHAVIOR OF MEDIUM-CR STEEL OIL AND GAS COLLECTING AND TRANSPORTING PIPELINE IN SIMULATED WORKING ENVIRONMENT*

Yang Gu[1]
Hui-bin Wu[2]
Rui Yuan[3]
Peng-cheng Zhang[4]
Zheng-zhi Zhao[5]
Shuai Song[6]

Abstract
The corrosion behavior of three kinds of medium-Cr rolled steel pipeline steels in carbon dioxide collecting and transporting environment at different temperatures was studied. The results shew that the 5Cr sample was most affected by temperature. When the temperature rised from 30 °C to 90 °C, the corrosion rate increased from 0.12 mm/a to 1.87 mm/a, which was increased 15.6 times. The corrosion rate of 7Cr steel at 30 °C was similar to that of 5Cr steel. However, as the temperature increased, the corrosion rate rised slowly, increasing by 2.4 times at 90 °C. The corrosion rate of 9Cr steel was not obvious with temperature, and it was always below 0.06 mm/a. The thickness of the corrosion product film of the three samples gradually increased below 70 °C, and suddenly increased above 70 °C. This was related to the negative temperature coefficient of the solubility of $FeCO_3$, and the thickening of the product film also affected the ion exchange of the cathodic reaction. An increase in the Cr content contributed to grain refinement and increased the proportion of the small-angle grain boundaries. More fine grains mean an increase in the total length of the grain boundaries, which could provide a diffusion channel for the free Cr element; on the other hand, the low-angle grain boundary structure was more orderly, with a lower free volume and lower interface energy. Under the combined effect of both, 9Cr steel and 7Cr steel had high volta potential and better corrosion resistance.
Keywords: Medium Cr steel; Carbon dioxide corrosion; Micro-area volta potential.

[1] *Master, student, Collaborative Innovation Center of Steel Technology, University of Science and Technology Beijing, Beijing, China.*
[2] *Doctor, researcher, Collaborative Innovation Center of Steel Technology, University of Science and Technology Beijing, Beijing, China.*
[3] *Master, student, Collaborative Innovation Center of Steel Technology, University of Science and Technology Beijing, Beijing, China.*
[4] *Doctor, negative researcher, Collaborative Innovation Center of Steel Technology, University of Science and Technology Beijing, Beijing, China.*
[5] *Doctor, researcher, Collaborative Innovation Center of Steel Technology, University of Science and Technology Beijing, Beijing, China.*
[6] *Bachelor student, Collaborative Innovation Center of Steel Technology, University of Science and Technology Beijing, Beijing, China.*

** Technical contribution to the 11th International Rolling Conference, part of the ABM Week 2019, October 1st-3rd, 2019, São Paulo, SP, Brazil.*

1 INTRODUCTION

For a long time, the severe corrosion caused by CO_2 remaining in the production liquid has occurred in the oil and gas transportation environment. Equipment damage and pipe perforation caused by corrosion are safety hazards and even give rise to serious accidents, but this problem has not received enough attention. As the exploitation of oil and gas fields enters the middle and late stages, the mining environment of the oil and gas fields is more severe, and the CO_2 corrosion problem of the facilities is more prominent. Therefore, many researchers have developed low-Cr pipeline steels to solve this problem and achieved good results[1-4].

Chen et al.[5] have shown that Cr easily forms $Cr(OH)_3$ under CO_2 environment. Since $Cr(OH)_3$ is weakly acidic, it can be stably present in a weakly acidic corrosive medium, and $FeCO_3$ will dissolve under the action of carbonic acid, resulting in enrichment of Cr content in the corrosion product film.

Xu Lining et al. [6] found that 3% Cr pipeline steel did not undergo local corrosion, and its average corrosion rate increased first and then decreased, and the peak temperature was around 100 °C. The corrosion product film of 3% Cr pipeline steel has two layers: the inner membrane is a dense Cr-rich layer, mainly composed of Cr-containing compounds and amorphous $FeCO_3$. And with the increase of temperature, the degree of Cr enrichment increases, the thickness of the inner layer film decreases; the outer layer film is formed by the accumulation of crystalline $FeCO_3$.

The study [7] found the corrosion kinetics changed at 60°C. And the solubility of ferrous carbonate ($FeCO_3$) has a negative temperature coefficient and decreases with increasing temperature. Therefore, between 60 °C and 110 °C, the steel surface can form a protective corrosion product film layer, which causes a transition zone of corrosion rate, and the local corrosion is prominent in this temperature region.

In the near stage, due to the high viscosity of heavy oil, the oil layer seepage resistance is large, and the oil production methods such as conventional water injection development are difficult to carry out effectively, which makes the mining difficult. Therefore, the oil and gas industry uses CO_2 to increase the oil recovery rate (Enhanced Oil/Gas Recovery, EOR/EGR) to prolong the life of oil wells[8, 9], followed by more serious corrosion problems. At present, there is limited research on the corrosion behavior of pipeline steel in the special environment of EOR, and there is no product development for special pipe for carbon dioxide flooding. In this paper, based on the low Cr alloy steel, the composition is further optimized, and the corrosion test and mechanism research are carried out, so as to provide reference data for the development of EOR/EGR pipe products.

2 MATERIAL AND METHODS

The experimental materials used in this paper are three kinds of rolled steels named Cr5, Cr7 and Cr9. The design of the steels adopt the principle of low carbon and microalloying, then added different levels of chromium. The measured element content is shown in Table 1 below. The experimental materials were smelted by vacuum smelting furnace. The casting blanks were forged with a process of opening at 1150 °C and final forging at 900 °C. The rolling was carried out in two stages after the steels were heated to 1200 ° C and kept for 2 h. The first stage was the rough rolling stage which starting temperature was 1100 °C, the second stage was the finishing rolling stage which starting temperature was 850 °C

A pre-formulated solution was used as the corrosion solution herein for corrosion accelerated testing and electrochemical testing. The composition of the corrosive

liquid is based on the actual environment production fluid configuration of an oil field. The ion content (in mg/L) of the corrosion test medium was as follows: HCO_3^- 4500, SO_4^{2-} 900, Mg^{2+} 150, Ca^{2+} 125, Cl^- 10000. According to the experience of an oil field, the oil transport environment conditions are temperature T=30~90 °C, carbon dioxide partial pressure P=0.5~2 MPa. Therefore, the corrosion accelerated testing was conducted at 30, 50, 70, 90 °C, with a rotating speed 160 r/min. The corrosion time was 120 h with a carbon dioxide pressure of 0.6 MPa.

Table 1. Elemental compositions of all the materials (wt.%).

No.	C	Cr	Si	Mn	P	S	Al	Ni	Cu	Nb	Fe
Cr5	0.037	5.42	0.3	0.53	0.005	0.013	0.058	0.30	0.28	0.02	Bal.
Cr7	0.047	7.58	0.3	0.34	0.005	0.0087	0.0033	0.21	0.26	0.02	Bal.
Cr9	0.048	8.41	0.32	0.22	0.005	0.0013	0.0038	0.17	0.27	0.02	Bal.

The tested steel was uniformly cut into coupons of 30 mm×10 mm×3 mm, and then a small hole of Φ4 mm was opened at a distance of 1 mm from the narrow edge of the hanging piece, and finally all the faces of the coupons were sanded from 200 to 800 mesh sandpaper in order. After completion of the coupons, they were washed with C_2H_6O and dried, and then weighed with an electronic balance to record the initial quality before the start of the experiment. Five parallel samples were set for each set of corrosion tests, two for surface and cross-sectional morphology observations and three for corrosion rate determination.

A chemical dissolution method was used to remove the corrosion layer; the corroded specimen was immersed in a vigorously stirred specific diluted HCl solution (500 mL HCl + 500 mL distilled water + 3.5 g hexamethylenetetramine) for at least 10 min at room temperature.

Afterward, the corrosion products were removed, rinsed, dried, and reweighed to obtain the final weight of the specimen. The corrosion rate was obtained by the following equation:

$$V=\frac{87600\times(M_0-M_t)}{SDT} \quad (1)$$

where V is the average corrosion rate (mm/a); M_0 and M_t are the original and final weights of the specimen (g), respectively; T is the immersion time (h); D is the steel density (g/cm^3); and S is the exposed surface area (cm^2).

The corrosion morphology of the samples was observed using a FEI-QUANTAFEG450 environmental scanning electron microscope. Pre-inlaying is required to observe the cross-section of the corrosion product, followed by sanding and polishing. The electrochemical specimens were welded with wires and then cold-sealed with epoxy to expose a 1 cm^2 surface for testing.

A three-pole potential system was used in the electrochemical test. The polarization curves were collected by a potentiodynamic sweep technique using a VersaSTAT MC electrochemical workstation. The tests were carried out at 30, 50, 70 °C respectively

Scanning kelvin atomic probe force microscope can detect the surface morphology and surface volta potential distribution at the same time. After cutting, grinding and polishing the test steels were immersed in 10% nitric acid for 90 s in an ultrasonic vibration environment to etch a better vision of morphology. After obtaining the SKPFM test sample, the surface morphology and surface volta potential distribution were simultaneously measured using an AFM-3D Infinity atomic force microscope from Oxford.

3 RESULTS AND DISCUSSION

3.1 corrosion rate

It can be seen from Figure 1 that the 5Cr sample was most affected by temperature. When the temperature rises from 30 °C to

90 °C, the corrosion rate increased from 0.12 mm/a to 1.87 mm/a, which was 15.6 times of 30 °C. Wherein the corrosion rate had a fastest increase within the interval of 50 °C to 70 °C. The corrosion rate of 7Cr sample was similar to that of 5Cr sample at 30 °C, however, the corrosion rate increases slowly with the increase of temperature. This increase was mainly reflected when the temperature is higher than 50 °C, while the change is not significant before 50 °C. The 9Cr sample was kept at a low level corrosion rate in this temperature range, which was always below 0.06 mm/a, and there was even a slight decrease at 90 °C.

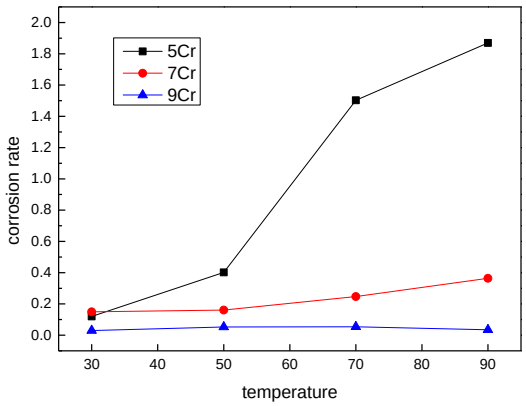

Figure 1. Curve of corrosion rate of three test steels with temperature

At 30 °C the surfaces of the three samples were covered by granular products, which were dense and uniform, shown in Figure 2 (a), (d), (g). The covered surface were also faintly visible in the scratches left over from the preparation, indicating a low degree of corrosion. The size of particles on the surface increased slightly with the increase of Cr content

It can be seen from Figure 2 (b), (e), (h) the product films of the three samples were both double-layered and the thicknesses were close. The thicknesses of the inner layer film of 5Cr and 7Cr steel were slightly thicker than that of the outer layer, and the inner and outer layers of 9Cr steel werre substantially equal in thickness. The substrate of the 5Cr sample was relatively flat and slightly uniform corrosion occurred. The 7Cr sample showed a large undulation, and there was uniform corrosion and pitting. The 9Cr sample was more pitting, and the pit depth was about 2 μm.

After the product film was removed from the 5Cr sample, a slight local uniform corrosion was observed on the surface, and the scratches at other locations were faintly visible, indicating that the degree of corrosion was light. The surface of the 7Cr sample was dominated by uniform corrosion, and uncorroded areas appear in some locations. The 9Cr sample showed clear scratches, pitting corrosion at some locations, and no uniform corrosion marks were found.

According to experience, the inner layer is a dense Cr-rich amorphous corrosion product with good protection, and the outer layer is $FeCO_3$. [2, 10, 11] And the products of medium-Cr steel are the same as those of low-Cr steel [12, 13]

As can be seen from Figure 3, the corrosion products of the three experimental steels formed at 70 °C consisted of a dense inner film and outer layer particles attached to the inner film. The inner film was evenly covered to cover the substrate. The inner film of 5Cr steel was severely damaged and incomplete. A large number of cracks appeared in the inner film of the 7Cr sample, however the coverage was relatively complete. The inner layer film of the 9Cr sample was well preserved, and even if it was taken out from the solution, it has a good protective effect on the substrate.

It can be seen from the cross-sectional view of the corrosion product that 5Cr was a uniform coating of the surface product film of the sample, and the thickness was large, but there was a large amount of gap in the film. The 7Cr and 9Cr sample product films were thin, and the granular outer layer were incompletely covered. At the same time, as the Cr content increased, the particles size increased.

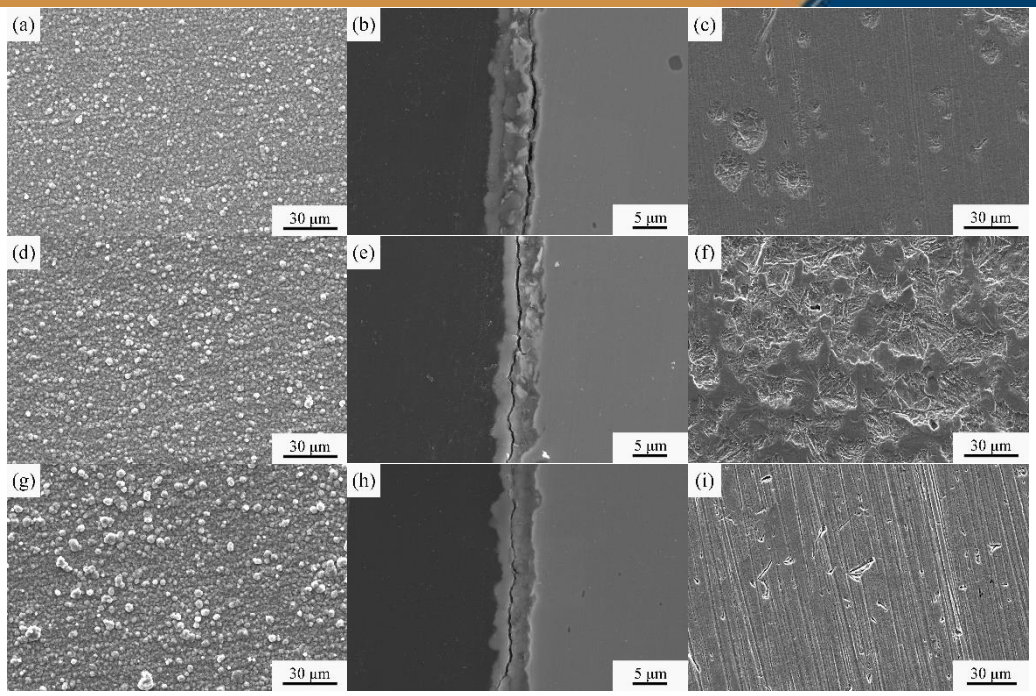

Figure 2. Corrosion morphology of three experimental steels at 30 °C **(a), (b), (c): 5Cr, (d), (e), (f): 7Cr; (g), (h), (i): 9Cr; (a), (d), (g): with corrosion product**

After removing the product film, it was found that the 5Cr sample was dominated by uniform corrosion and less pitting. The 7Cr and 9Cr samples showed clear scratches, pitting corrosion at some locations, and no uniform corrosion marks were found. Pitting corrosion of 9Cr samples was more serious than 7Cr.

It can be seen from the Figure 4 that the corrosion products of the 5Cr and 7Cr test steels at 90 °C were similar to those of other temperatures, with a dense protective film from the inner layer and a granular product distributed above the inner layer film. At the same time, the cracking of the inner film was reduced. The corrosion product of the 9Cr sample appeared to consist of a single layer film, and no particulate deposits were observed on the surface.

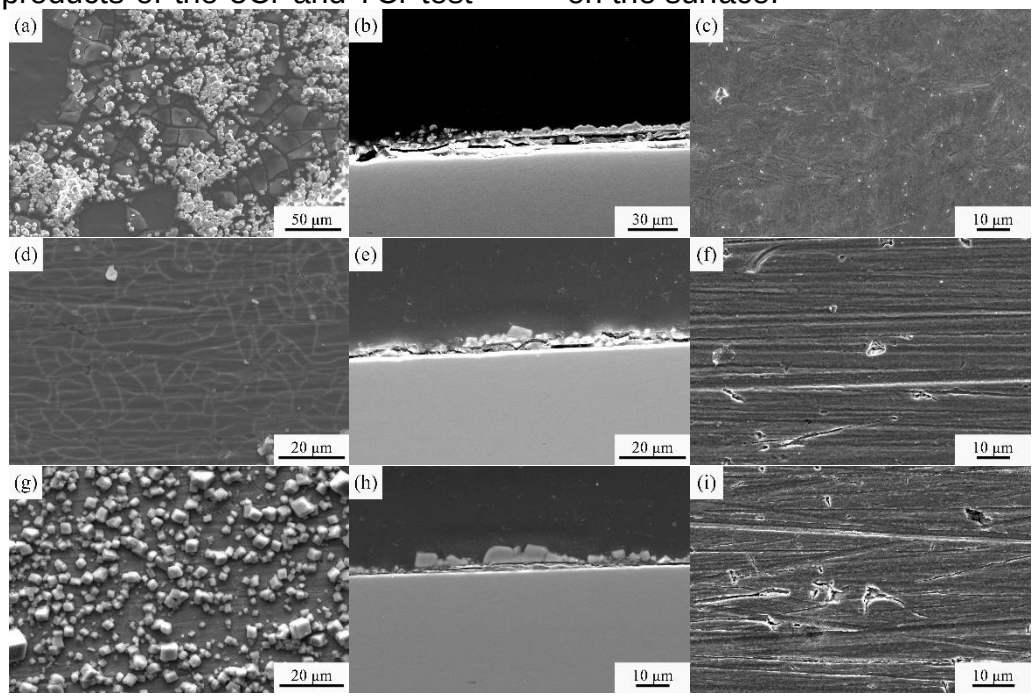

Figure 3. Corrosion morphology of three experimental steels at70 °C (a), (b), (c): 5Cr, (d), (e), (f): 7Cr; (g), (h), (i): 9Cr; (a), (d), (g): with corrosion product

The cross section of the 5Cr sample can be seen, the corrosion product consists of three parts, the innermost layer was a loose mixed product, the middle layer was a dense film, and the outer layer was a granular product. The corrosion product of the 7Cr sample consisted of an uneven in thickness inner mixed layer and outer granular product. The corrosion product of the 9Cr sample consisted of a mixed monolayer film of uniform thickness. And, it was found that the surface of the test steels were flat under the protection of corrosion products, and no obvious local corrosion occurred.

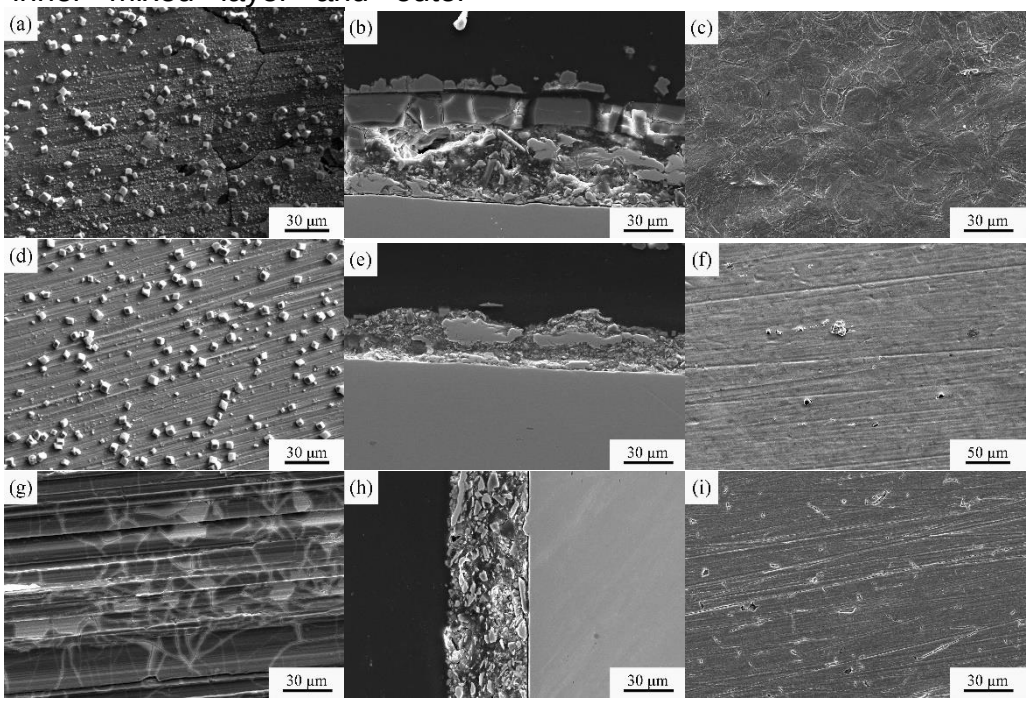

Figure 4. Corrosion morphology of three experimental steels at90 °C (a), (b), (c): 5Cr, (d), (e), (f): 7Cr; (g), (h), (i): 9Cr; (a), (d), (g): with corrosion product

When the product film was removed, it was found that the 5Cr sample had severe general corrosion, and the 7Cr sample had a slight general corrosion, and the 9Cr sample had a slight pitting.

It can be seen from the Figure5 that the film thickness of the corrosion products of the three samples at 30 °C is thin and the differences were not large, all of which were about 6 μm. At 70 °C, the thickness of 7Cr and 9Cr samples did not increase much, but the thickness of 5Cr sample began to be significantly higher than the other two groups. At 90 °C, the corrosion product film of the three samples suddenly thickened, while the thickness of the 5Cr sample was close to 75 μm much larger than the other two samples, and the 7Cr and 9Cr samples were about 36 μm and 48 μm, respectively. this phenomenon was related to the negative correlation between the solid solubility and temperature of $FeCO_3$ [14].

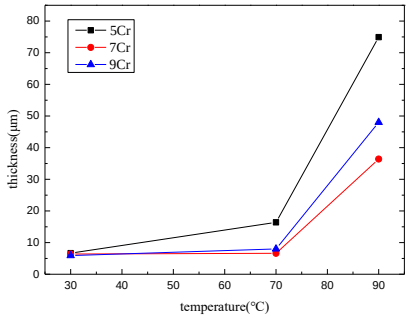

Figure 5. Curves of film thickness of corrosion products of three kinds of experimental steels with temperature

3.2 Polarization curve

It can be seen from the Figure 6(a) that at 30 °C as the Cr content increased, the corrosion potential gradually increased, and the corrosion current gradually decreased. The cathodic polarization

curves of the three samples were similar in shape, indicating that the reaction mechanisms are the same. The anodic polarization curve of 9Cr sample was different from that of 5Cr and 7Cr, and a relatively obvious passivation platform appears, which indicates that 9Cr steel has excellent corrosion resistance. Although the 5Cr and 7Cr steel did not have a passivation platform, an inflection point appears in the high current density region, indicating that the appearance of the corrosion product film also protected the substrate.

At 50 ° C, the polarization curves of the three samples showed the same trend as 30 °C. As shown in Figure 6(b), the difference was that the passivation platform of 9Cr steel disappeared and was replaced by semi-passivation behavior. Study found that the semi-passivation behavior also protects the substrate [15].

From Figure 6(c),it can be seen that the cathode reaction at 70 °C fluctuated greatly compared with the low temperature. Analysis the reason is this phenomenon was related to the thick corrosion products, and the thick corrosion products affected ion exchange in the solution [16]. The corrosion product film had cation selectivity that hinders ion exchange during the reaction, thus resulting in a lower corrosion rate of the test steel.

3.3 EBSD test

The Figure 7 showen the orientation distribution map and grain boundary distribution diagram of three kinds of experimental steels. And Figure 8 show the orientation difference angle ratio map and the grain size ratio map prepared after the statistics were calculated. According to the calculation of the grain size, the average grain size of 5Cr sample was 2.69 μm, 7Cr sample was 2.07 μm and 9Cr sample was 1.98 μm. It can be seen that the grain size decreased with the increase of Cr content. As a result, the decrease of grain size increased the number of grain boundaries, and the Cr element tended to be segregated or precipitated at the grain boundary. At the same time, the higher energy of the grain boundary also provided a channel for the diffusion of Cr element.

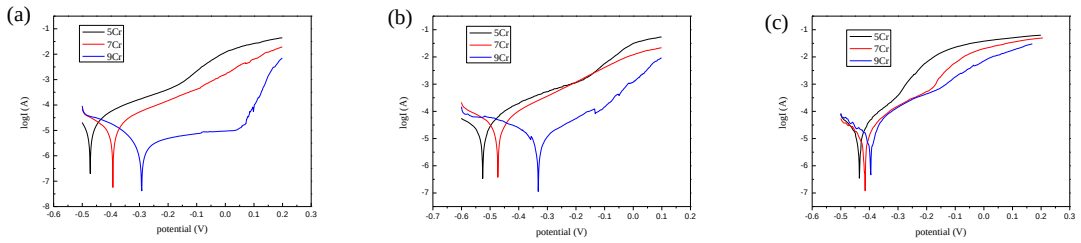

Figure 6. Polarization curves of three test steels at different temperatures (a) 30 °C; (b) 50 °C; (c) 70 °C

Table 2. Polarization curve fitting data

Steel	Temperature	Ecorr(mV)	Icorr(mA)	βa(mV/dec)	βc(mV/dec)
5Cr	30	-474.576	5.449	53.3	43.8
	50	-524.002	18.121	96.7	157.6
	70	-432.518	11.710	83.5	87.4
7Cr	30	-390.389	8.577	94.1	139.4
	50	-462.904	21.944	82.2	154.1
	70	-411.466	10.297	65.1	125.8
9Cr	30	-299.783	1.228	132.5	48
	50	-319.009	11.373	173.5	236.4
	70	-405.027	14.637	95.7	135.2

Studies [17] have shown that the increasing of Cr content can increase the proportion of low-angle boundaries, while the proportion of high-angle boundaries decreases, and the density of dislocations increases. This is because the solid solution of Cr in Fe reduces the stacking fault energy of steel, which causes a large number of low-energy intragranular interfaces in the steel during thermal

deformation. At the same time, the migration of the grain boundary is pinned, which hinders the penetration of high-angle boundaries [18]. It can be seen from the Figure 8 that the grain boundary types of the three experimental steels were mainly low-angle boundaries, the low-angle boundary ratio of the 5Cr sample was 56.4%, the 7Cr sample was 65.15%, and the 9Cr sample was 62.9%. The low-angle boundary ratio in this experiment did not increase strictly with the increase of Cr content, but the increase of Cr content was beneficial to the increase of low-angle boundaries.

High-angle boundaries are more prone to corrosion due to higher energy and are prone to corrosion initiation and development. The reason is that the initiation and development of corrosion often occur at high energy locations [19]. Since the grain boundaries are the main defects of the crystal structure, the energy is higher and the corrosion tendency is greater at these locations. Due to the highly ordered structure, the small-angle grain boundary has a small free volume and low interfacial energy, which can interrupt the connectivity of high angle boundaries and effectively block the expansion of corrosion along a large angle [20].

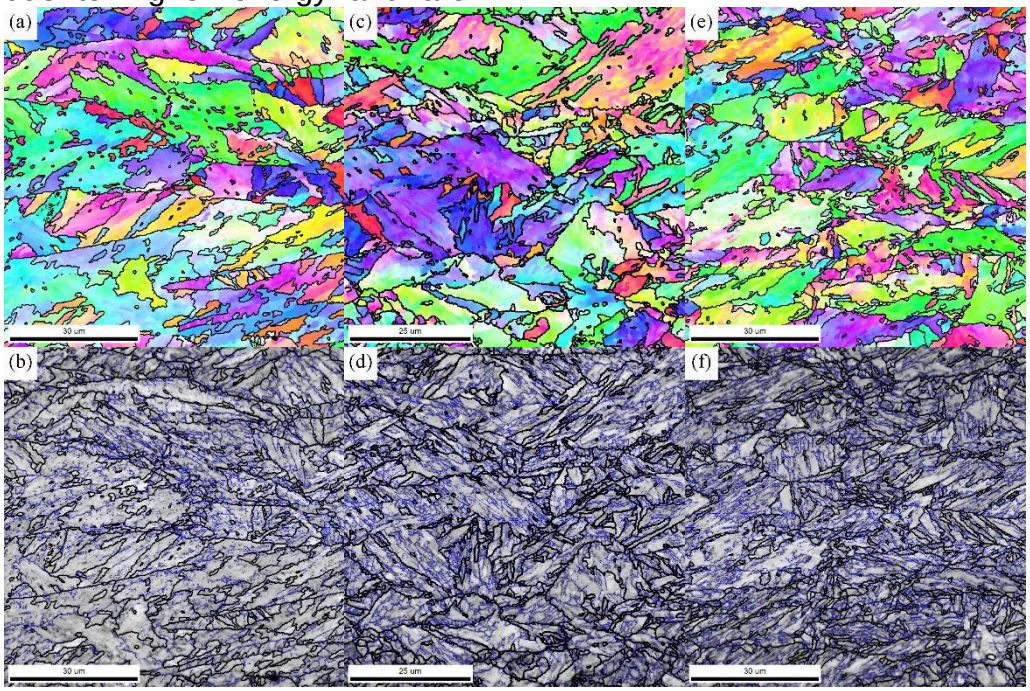

Figure 7. EBSD test results (a), (b): 5Cr; (c), (d): 7Cr; (e), (f): 9Cr; (a), (c), (e) grain orientation map ; (b), (d), (f) grain boundary distribution map

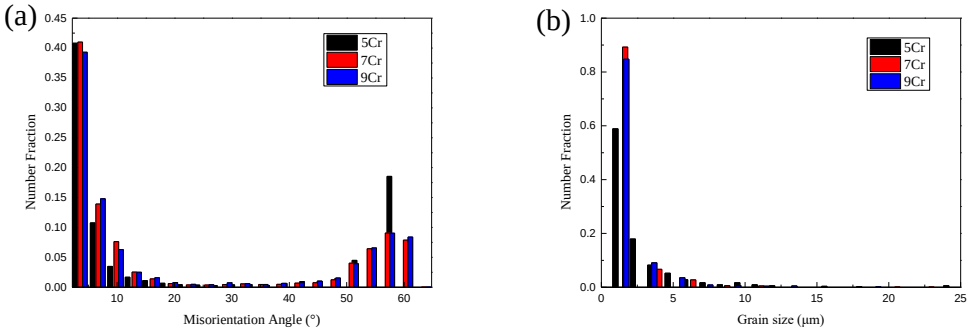

Figure 8. EBSD statistical results (a) grain boundary angle distribution map (b) grain size distribution map

3.4 Microscopy Volta Potential

It can be seen from the Figure 9 that the highest volta potential of the 5Cr sample in

this region was 947.8 mV, the lowest was -503.5 mV; the highest volta potential of the 7Cr sample was 2.123 V,and the lowest was -472.3 mV; the highest volta potential of the 9Cr sample was 1.958. V, the lowest was -635.8mV.

As the Cr content increased, the high volta potential rised from about 1V to about 2V,which is consistent with the previous studies [21, 22] that the increase in Cr content contributes to the improvement of corrosion resistance.

In addition, since the minimum potentials did not change much, from the superficies,the volta potential difference increased, the corrosion driving force increased [23, 24, 25]. However, as shown in Figure 8. (d), (f), the points where the high potential exists in the 7Cr and 9Cr test steels were individual high points. As the Cr content increased, the number of individual high points decreased, and the volta potential value of the special point increased. The phenomenon was particularly evident on the 9Cr sample. It is speculated that the risk of pitting corrosion increases as the Cr content increased [18].

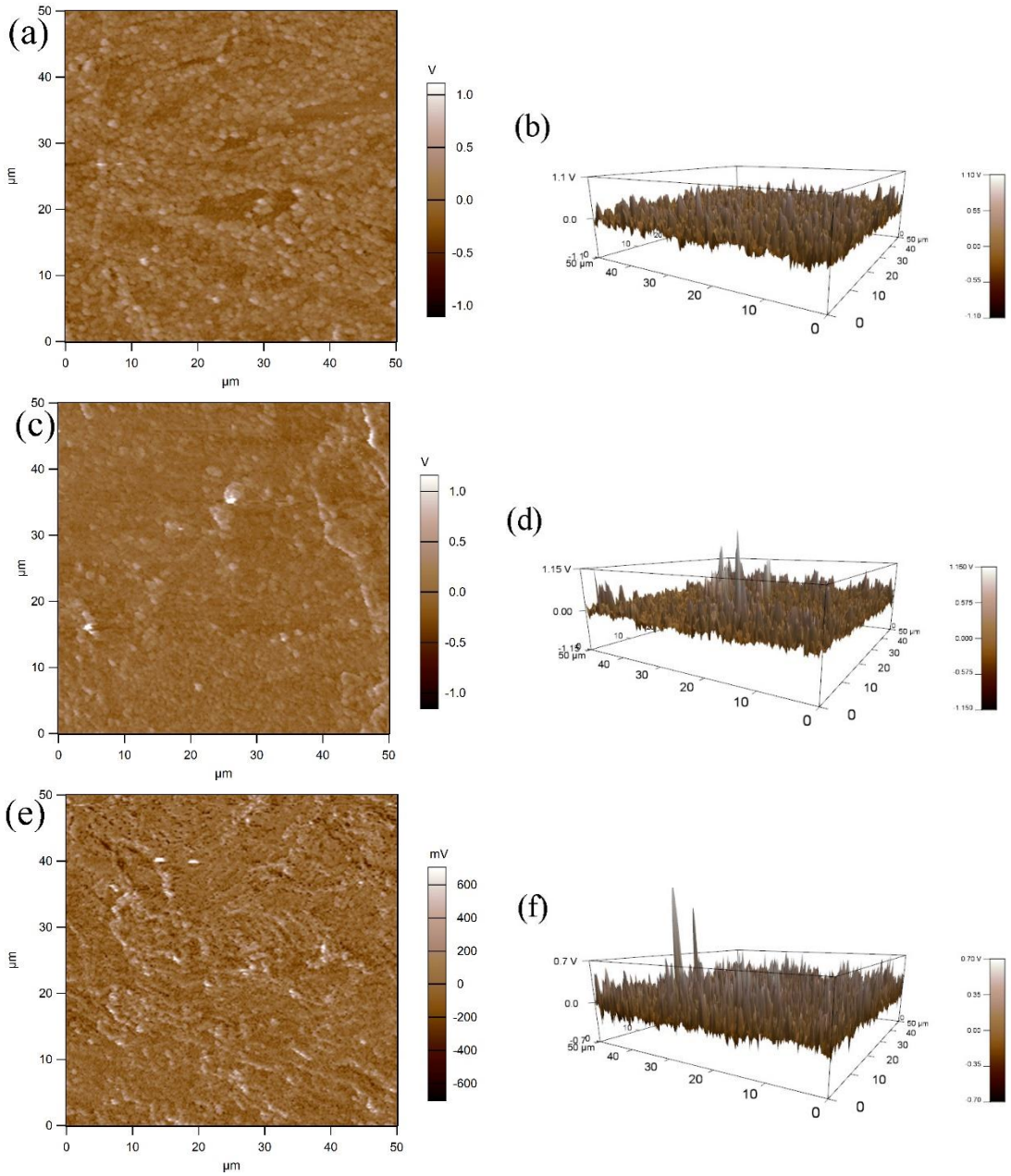

Figure 9. Micro-zone volta potential distribution maps of three test steels (a), (b): 5Cr; (c), (d): 7Cr; (e), (f): 9Cr; (a), (c), e): 2D; (b), (d), (f): 3D

Select a typical area for further analysis of the volta potential difference of the micro-areas. These areas were taken from Figure 9. For the specific position, refer to the position coordinates of the side and the bottom of the figures. The selected area was 10 μm, and there was no particular point in the uniform arrangement of the grains in the area. In this region, the volta potential change at the position of the red line was analyzed, and the red line crossed a plurality of crystal grains. The curve of the 5Cr sample shows that there were about 6 crystal grains at the scribe line, and the crystal grains were approximately circular equiaxed crystals, and the volta potential dropped significantly at the grain boundary. The intragranular volta potential was high and the volta potentials between the crystal grains were similar. The volta potential value changed high and low in order, and the volta potential fluctuates between ±0.2 V. The 7Cr and 9Cr samples had about 6-7 crystal grains passing through the red line. The volta potential differences between different crystal grains were large, and the volta potential distributions were not uniform. In most cases, the volta potential fluctuates within a small range, and the 7Cr sample was about ±0.1 V. The 9Cr sample fluctuated within a range of less than ±0.1 v. The volta potential change did not strictly change with the distribution of crystal grains. This characteristic reaction should be mitigated by uniform corrosion at the macro level and localized corrosion is aggravated.

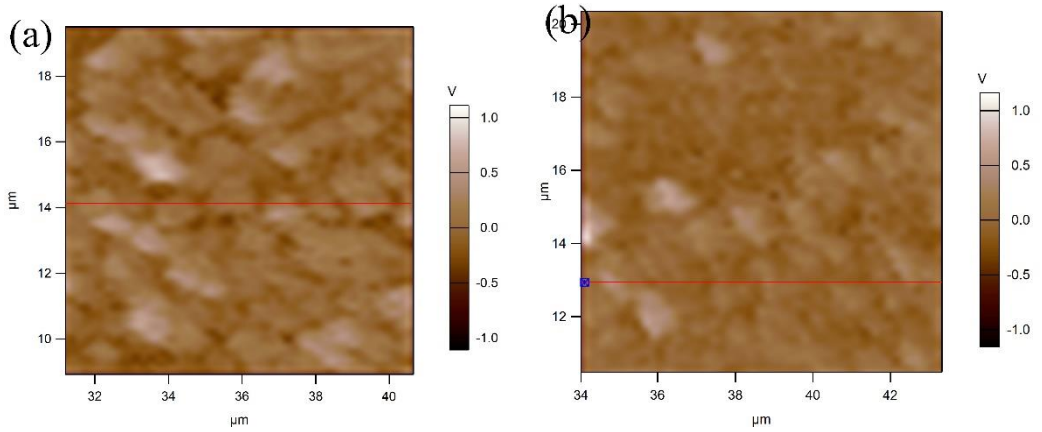

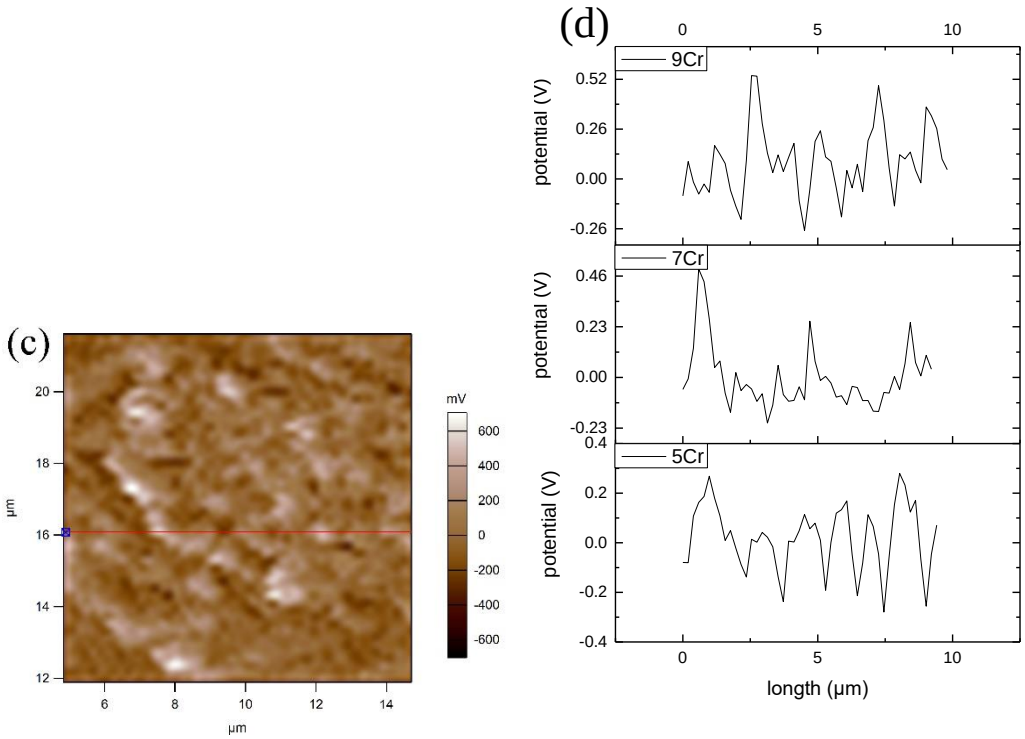

Figure 10. Statistical graph of local micro-region volta potential (a): 5Cr selected area; (b): 7Cr selected area; (c) 9Cr selected area; (d) Volta potential trend

4 CONCLUSION

1. The 5Cr sample was most affected by temperature. When the temperature rised from 30 °C to 90 °C, the corrosion rate increased from 0.1201 mm/a to 1.8698 mm/a, which was 15.6 times. The corrosion rate of 7Cr steel at 30 °C was similar to that of 5Cr steel. With the increased of temperature, the corrosion rate rised slowly, and it was 2.4 times at 90 °C. The corrosion rate of 9Cr steel was not obvious with temperature, and it was always around 0.06 mm/a. The thickness of the corrosion product film of the three samples gradually increased below 70 °C, and suddenly increased at 90 °C. However, the corrosion resistance of 9Cr steel had not been affected by temperature and film thickness, and had been at a good level.
2. The corrosion mechanism of the three experimental steels had slightly different between 30 °C and 70 °C. 9Cr steel had obvious passivation platform at 30 °C, and semi-passivation occurd at 50 °C. At 90 °C, the cation selectivity of the product film hinderd ion exchange, and steel matrix was well protected as other temperaturs.
3. The increase of Cr content helped to refine grains and increased the proportion of low-angle grain boundaries, which can provide diffusion channels for free Cr element; on the other hand, the low-angle grain boundary structure was more orderly, with smaller free volume and the lower interface energy enhanced the corrosion resistance of the steels.
4. The increase in Cr element helped to increase the maximum volta potential of the experimental steels while increasing the volta potential difference.As a result the test steel was shown to be resistant to uniform corrosion, but it also increased the risk of pitting corrosion.

Acknowledgments

This work was financially supported by the National Key R and D Program of China (No. 2017YFB0304900).

REFERENCES

1 Li W, Xu L, Qiao L, et al. Effect of free Cr content on corrosion behavior of 3Cr steels in a CO_2 environment. J Applied Surface Science. 2017, 425(15): 32-45.

2 Guo S, Xu L, Zhang L, et al. Characterization of corrosion scale formed on 3Cr steel in CO_2 -saturated formation water J Corrosion Science. 2016, 110: 123-133.

3 Guo S, Xu L, Zhang L, et al. Corrosion of alloy steels containing 2% chromium in CO2 environments J Corrosion Science. 2012, 63: 246-258.

4 DU Zhiyong Liu Jin Gao Xiaogang Li Z J C. Effect of calcium ions on CO_2 corrosion of 3Cr low-alloy steel. J Acta Metallurgica Sinica(English letters). 2011, 24(5): 373-380.

5 Chen C, Lu M, Zhao G, et al. Characteristics of CO_2 Corrosion Scales On 1%Cr-Containing N80 Steel. J Journal of Chinese Society for Corrosion and Protection. 2003, 23(06): 11-15.

6 Xu L, Chen T, Chang W, et al. Effect of temperature on CO_2 corrosion production scales on 3%Cr pipeline steel. J Journal of University of Science and Technology Beijing. 2012, 34(02): 149-156.

7 Xiang Y, Xu M, Choi Y. State-of-the-art overview of pipeline steel corrosion in impure dense CO_2 for CCS transportation: mechanisms and models. J Corrosion Engineering, Science and Technology. 2017, 7(52): 485-509.

8 Oldenburg C M, Stevens S H, Benson S M. Economic feasibility of carbon sequestration with enhanced gas recovery (CSEGR). J Energy. 2004, 29(9-10): 1413-1422.

9 Shaw J, Bachu S. Screening, evaluation, and ranking of oil reservoirs suitable for CO_2-flood EOR and carbon dioxide sequestration. J Journal of Canadian Petroleum Technology. 2002, 41(09): 51-61.

10 Xu L. Wang b, Lu M, et al. Corrosion Behavior Of 6.5%Cr Steel In High Temperature And High Pressure CO_2 Environment. J Acta Metallurgica Sinica. 2016, 52(6): 672-678.

11 Guo S, Xu L, Chang W, et al. Experimental Study of CO_2 Corrosion of 3Cr Pipe Line Steel. J Acta Metallurgica Sinica. 2011, 47(8): 1067-1074.

12 Hua Y, Barker R, Neville A. The effect of O_2 content on the corrosion behaviour of X65 and 5Cr in water-containing supercritical CO_2 environments. J Applied Surface Science. 2015, 356(30): 499-511.

13 Liu Z, Gao X, Li J, et al. Corrosion behaviour of low-alloy martensite steel exposed to vapour-saturated CO_2 and CO_2 -saturated brine conditions. J Electrochimica Acta. 2016, 213(20): 842-855.

14 Kermani M B, Morshed A. Carbon dioxide corrosion in oil and gas production—a compendium. J Corrosion. 2003, 59(8): 659-683.

15 Xu L, Zhu J, Wang B. Influence of Cr Content and pH Value on the Semi-Passivation Behavior of Low Cr Pipeline Steels. J Acta Metallurgica Sinica. 2017, 53(06): 677-683.

16 Luo B, Zhou J, Bai P, et al. Comparative study on the corrosion behavior of X52, 3Cr, and 13Cr steel in an O_2–H_2O–CO_2 system: products, reaction kinetics, and pitting sensitivity. J International Journal of Minerals, Metallurgy, and Materials. 2017, 24(6): 646-656.

17 X Wang, Y Chen, G Niu, et al. The study on corrosion resistance of high-strength spring steel. J Corrosion Engineering, Science and Technology. 2018, 53(1): 54-64.

18 Liang J, Tang D, Wu H, et al. Corrosion Behaviors of Cr Low-Alloy Steel in Bottom Plate Environment of Cargo Oil Tanks. J Journal of South China University of Technology (Natural Science Edition)). 2013, 41(10): 72-78.

19 Wu H B, Wu T, Niu G, et al. Effect of the frequency of high-angle grain boundaries on the corrosion performance of 5wt%Cr steel in a CO_2 aqueous environment. J International Journal of Minerals Metallurgy and Materials. 2018, 25(3): 315-324.

20 Song D, Ma A B, Jiang J H, et al. Corrosion behaviour of bulk ultra-fine grained AZ91D magnesium alloy fabricated by equal-channel angular pressing. J Corrosion Science. 2011, 53(1): 362-373.

21 Liang J, Tang D, Wu H, et al. Environment corrosion behavior of cargo oil tank deck made of Cr-contained low-alloy steel. J Journal of Southeast

University (Natural Science Edition). 2013, 43(01): 152-157.
22 Gu Y, Wu H, Yuan R, et al. Influence of Cr content on corrosion performance of middle Cr alloy steel in CO_2 environment J Materials Research Express. 2019, 6(4): 46511.
23 örnek C, Engelberg D L. SKPFM measured Volta potential correlated with strain localisation in microstructure to understand corrosion susceptibility of cold-rolled grade 2205 duplex stainless steel. J Corrosion Science. 2015, 99: 164-171.
24 Sathirachinda N, Pettersson R, Pan J. Depletion effects at phase boundaries in 2205 duplex stainless steel characterized with SKPFM and TEM/EDS. J Corrosion Science. 2009, 51(8): 1850-1860.
25 Guo L Q, Li M, Shi X L, et al. Effect of annealing temperature on the corrosion behavior of duplex stainless steel studied by in situ techniques. J Corrosion Science. 2011, 53(11): 3733-3741..